Journal of Membrane Science 680 (2023) 121732

Contents lists available at ScienceDirect

Journal of Membrane Science

journal homepage: www.elsevier.com/locate/memsci

Amine-functionalized biogenic silica incorporation effect on poly (ether-block-amide) membrane CO_2/N_2 separation performance

Wahyu Kamal Setiawan, Kung-Yuh Chiang *

Graduate Institute of Environmental Engineering, National Central University, No. 300, Chung-Da Road., Chung-Li District, Tao-Yuan City, 32001, Taiwan

ARTICLE INFO

Keywords:
Pebax 1657
Amine
Biogenic silica
CO_2 separation

ABSTRACT

The development of eco-friendly filler materials in membrane-based gas separation technology have become fascinating science that has established a tremendous circular economy. Biogenic silica (BSi) was recovered from rice husks and functionalized using three different molecular structure amine groups in this study. Polyethyleneimine/PEI, N-methylaminopropyl trimethoxysilane/MAPS, and 2-(2-pyridyl) ethyltrimethoxysilane/PETS are used as inorganic fillers for the fabrication of poly (ether-*block*-amide) (Pebax-1657) mixed matrix membranes (MMMs). The amine functionalized silica and Pebax chains were found to interact through intermolecular hydrogen bonding, tightening the interfacial space and strengthening the thermal stability of the original polymeric membranes. Moreover, the amine groups in each functionalized BSi were sufficient to establish a facilitated transport mechanism for CO_2 through the Pebax membranes. Amine functionalized BSi could remarkably upgrade the CO_2 permeability (110–120%) and CO_2/N_2 selectivity (60–70%), surpassing Robeson's upper bound 2008. In addition, Pebax/BSi-MAPS-10 became the most reliable membrane in this study, with CO_2 permeability of 90.05 Barrer and CO_2/N_2 selectivity of 100.41. These findings revealed that amine functionalized BSi was promising for the fabrication of high-quality Pebax MMMs for CO_2/N_2 separation in industrial applications.

1. Introduction

Rising atmospheric CO_2 has consistently become a threatening issue for 1.5 °C global warming, primarily due to large-scale combustion and manufacturing processes in industrial activities. A recent report by NOAA's Global Monitoring Lab revealed a new record global average atmospheric carbon dioxide of 414.72 parts per million, jumping 2.58 ppm over 2021, despite the economic crisis during the COVID-19 pandemic [1]. This implied that massive CO_2 generation was inevitable due to society's high demand for energy, materials, and chemicals. Therefore, developing an advanced CO_2 separation and recycling technology is necessary to avoid severe catastrophic effects.

Among the CO_2 separation methods, membrane technology has received tremendous attention due to its inexpensive installation, simple operation, lean energy consumption, and less environmental impact [2]. Polymeric membranes are preferable, offering high gas separation efficiency with economic and ecological benefits [3]. Poly (ether-*block*-amide), a block copolymer, is a polymer option having both hard rigid segments (polyamide), which give mechanical strength, and soft flexible-chain blocks (polyethylene) that provide high permeability [4–6]. Pebax 1657, containing 60% PE, has been reported to present top acid gas separation performance [7] due to its high durability, flexibility, thermal resistance, mechanical strength, and remarkable selectivity for acid gas and polar–nonpolar gases [8]. However, despite the excellent Pebax 1657 separation performance, it has problems surpassing the Robeson upper bound curves, confirming a trade-off relationship between permeability and selectivity.

Mixed matrix membranes (MMMs) have been promoted as choice to achieve desired gas separation performances. The general idea for synthesizing MMMs is to induce the thermal, electrical, mechanical, and molecular sieve properties of inorganic materials into a polymer matrix [9]. Incorporating fillers with molecular sieving properties in the polymer matrix can lead to higher permeability, selectivity, or both over pure polymeric membranes. Among the numerous inorganic filler materials, silica is one of the most favorable options regarding its high mechanical and thermal stabilities, specific surface area, and flexibility for chemical functionalization [10,11]. The utilization of biogenic silica (BSi) derived from crop residues is a promising idea amid the increased

* Corresponding author.
E-mail address: kychiang@ncu.edu.tw (K.-Y. Chiang).

https://doi.org/10.1016/j.memsci.2023.121732
Received 29 January 2023; Received in revised form 30 April 2023; Accepted 8 May 2023
Available online 16 May 2023

use of chemical silica precursors such as tetraethyl orthosilicate (TEOS) and tetra methoxy silicate (TMOS) [12–14]. Rice husk based BSi will be preferable, considering its high abundance and raw material silica yield [15]. A recent report by Waheed et al. [14], even though, found an 85% improvement in the CO_2 permeability of polysulfone membranes by incorporating 40 wt% rice husk based BSi. This study highlighted the pore channels on the BSi surface, creating sufficient membrane gas diffusion pathways for CO_2. BSi could not perfectly hamper the trade-off issue of gas permeability-selectivity corresponding to non-selective voids formation within the membranes. Therefore, considerable opportunities exist for developing high-performance BSi fillers to destroy the prevalent problem of polymeric membranes.

Surface modification with a particular functional group, such as amine, improve the inorganic filler's ability to enhance polymeric membranes. The amine groups could render abundant carriers to facilitate polar gas transport through reversible reaction and simultaneously improve the filler–polymer interface compatibility [16]. Recent studies investigated the effects of amine-functionalized fillers for improving the CO_2 separation efficiency of Pebax membranes. Meshkat et al. [17] found a 174% improvement in CO_2 permeability over the neat Pebax using 10 wt% NH_2-MIL-53 as a dispersed phase. Likewise, Ding et al. [18] revealed that NH_2-ZIF-8 could enhance CO_2 permeability at 53% and 107.6% compared to ZIF-8/Pebax MMM and pure Pebax membrane. Amine groups in MIL-101 were also found to upgrade the CO_2 selectivity of Pebax membranes up to 145.1% [19]. No comparably investigated different amine groups functionalized on the filler surface were found to increase Pebax membrane CO_2 separation factors. This work investigates for the first time the ability of different molecular structured amines (linear, branched, and cyclic) on the rice husk-derived biogenic silica surface to improve the CO_2 separation performance of Pebax membranes. The results will benefit broadening the application of functionalized biogenic fillers for membrane-based CO_2 separation.

2. Experimental

2.1. Materials

Biogenic silica (BSi) was obtained by the process described elsewhere [20]. Pebax-1657 (Arkema, France), branched polyethyleneimine (PEI, 800 Mw, Sigma Aldrich), N-methylaminopropyl trimethoxysilane (MAPS, 95%, ACS grade, Alfa Aesar), 2-(2-pyridyl) ethyltrimethoxysilane (PETS, 95%, ACS grade, Gelest), and anhydrous ethanol (C_2H_5OH, 99.99%, ACS grade, J.T. Baker) were used as received.

2.2. Amine functionalization of filler

The amine functionalized BSi was prepared via a sonication method adapted from previous work [21]. One mmol amino silane was combined with ~0.5 g samples of RHS in 25 ml anhydrous ethanol. This mixture was then sonicated at 55 °C for 2 h. The mixture was then vacuum dried at 70 °C for 10 h to obtain amine-functionalized silica.

2.3. Membrane preparation

Pebax-1657 MMMs were fabricated as follows, 4 wt % polymeric solutions were first prepared by dissolving a polymer pellet into H_2O/EtOH (30/70 wt%) mixture at 70 °C for 2 h. Different fillers were then incorporated into the polymer solution at 10 wt% load and refluxed for another 2 h. The mixture was then cast into a PTFE Petri dish and ambient dried for 48 h, followed by vacuum drying at 50 °C overnight. The MMM thickness was controlled at 100–130 μm.

2.4. Characterization

Fourier-transform-infrared spectroscopy (FTIR) analysis was performed using an FTIR spectrometer PerkinElmer (Waltham, MA, USA) coupled with Deuterated Triglycine Sulphate (DTGS) detector to investigate the filler and prepared membrane functional groups and chemical composition. The optical system with a KBr beam splitter in FTIR was performed at 650–4000 cm^{-1} at a high resolution of 0.4 cm^{-1}. In addition, the functionalized filler organic elemental composition was measured using an elemental analyzer (Elementary Analyzer, Vario MICRO).

The membrane morphology was investigated using a Field emission scanning electron microscope (FESEM, Bruker Ultra-High Resolution FESEM). To obtain precise cross-section angle observation, the membranes were fractured cryogenically in liquid nitrogen and then top-coated with Au under vacuum conditions.

The filler and membrane semi-crystalline structures were characterized using X-ray diffraction (XRD, Bruker D8 Advance) with Cu Kα radiation (λ = 1.5406 Å), current voltages of 40 kV and 40 mA, scanning speed of 0.1 °C/s at 2θ = 10–90°. Bragg's law calculated polymer chain spacing (d-spacing) from XRD. Related data pattern analysis and calculations were performed using X'Pert HighScore software.

The Brunauer Emmett Teller (BET) surface area and Barrett-Joyner-Halenda (BJH) filler plots were obtained using a Micromeritics ASAP 2020 V3·00H system. Before measurements the samples were degassed under low pressure for 4 h at 120 °C.

The MMM thermal degradation behavior was studied using a thermal analyzer (HITACHI TG/DTA 7300). Three to four mg of MMM cut pieces were placed into a ceramic pan crucible, heated from 40 °C to 800 °C at 10 °C/min under 100 ml/min N_2.

Differential scanning calorimetry (DSC, MATTLER DSC 3) was used to determine the membrane glass transition temperatures (T_g). Samples were tested under N_2 atmosphere, with the temperature ranging from −60 °C to 250 °C at 10 °C/min.

The membrane mechanical properties were determined using a tensile tester equipment (A&D MCT-2150) with a testing speed of 70 mm/min. The measurement was repeated three times to obtain the standard deviation.

2.5. Gas permeation test

The single gas permeation membranes were measured using custom permeation equipment using the constant volume/variable pressure method, as seen in Fig. 1.

Before each test the membrane samples were vacuum treated overnight. The membrane sample was placed onto a permeation cell. The effective permeation area was 3.069 cm^2. Both feed and permeate sides were consequently evacuated from the remained unexpected gases. Feed gas (CO_2/N_2) was then introduced steadily into the inlet side of the membrane cell with the outlet valve closed until the gauge reached the required pressure. The permeate flow rate was recorded by monitoring the mass flow meter as steady state conditions appeared. CO_2 and N_2 permeation analyses were evaluated at ambient temperature under varied pressures (1, 2, 3, 4, 5 bar). Each test was repeated three times to get the average and standard deviation.

The gas permeability, P (1 Barrer = 10^{-10} cm^3 STP $cm{\cdot}cm^{-2}s^{-1}cmHg^{-1}$) was determined using the following equation:

$$P = 10^{10}\frac{Q \times l}{\Delta P \times A} \quad (1)$$

where Q is the gas permeation flow (cm^3/s STP), l is the membrane thickness (cm), A is the effective area (3.069 cm^2), and ΔP is the transmembrane partial pressure difference (cmHg). The ideal CO_2/N_2 selectivity was determined using the equation:

$$\alpha_{CO_2/N_2} = \frac{P_{CO_2}}{P_{N_2}} \quad (2)$$

where P_{CO2} and P_{N2} are the permeability of CO_2 and N_2, respectively.

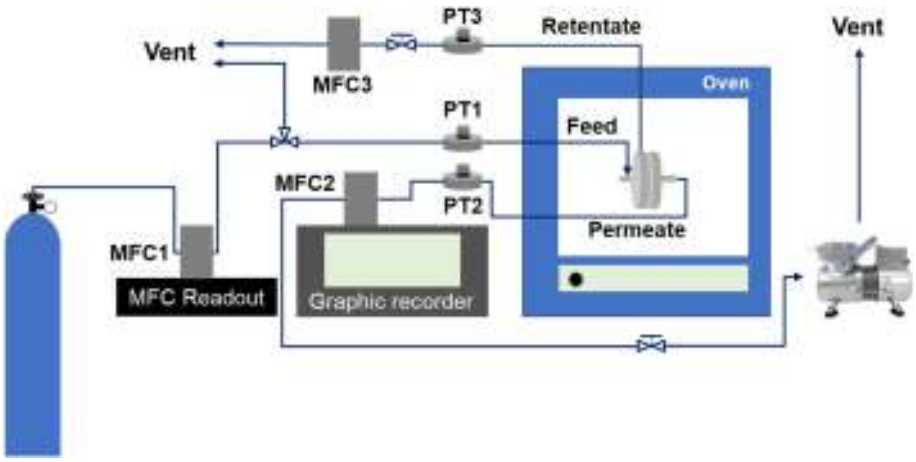

Fig. 1. Single gas permeation system for measuring CO_2 and N_2 permeabilities.

Permeability enhancement ratio (PER) and selectivity enhancement ratio (SeER) were calculated to evaluate the ability of filler to improve separation fixtures of Pebax membranes, following the formulas below:

$$PER_{CO2} = (P_{MMM} - P_{neat}) / P_{neat} \quad (3)$$

$$SeER_{CO2/N2} = (\alpha_{MMM} - \alpha_{neat}) / \alpha_{neat} \quad (4)$$

3. Results and discussion

3.1. Filler characterization

The interaction between biogenic silica with three different amines was demonstrated through comparative Fourier transform infrared spectroscopy (FTIR) analyses, as seen in Fig. 2. All samples showed absorption bands at 1050-1100 cm^{-1} and 790-800 cm^{-1}, which were assigned to Si–O–Si asymmetric stretching and Si–O–Si symmetric stretching [22]. However, the wide band at 3400 cm^{-1} attributed to anti-symmetrical stretching vibration from –OH was observed only in the BSi sample attributing its hydrophilic characteristic. On the other hand, weak peaks were observed at 1650–1590 cm^{-1} for the all-functionalized BSi, corresponding to the bending vibration of N–H [23]. In addition, the broad stretching band in the range of 3300–3500 cm^{-1} was dedicated to the NH_2 group [10]. Therefore, the observed amine peaks confirmed the successful functionalization of BSi particles.

The XRD peaks of amine functionalized BSi filers were identical with unmodified BSi (Fig. 2b), displaying the amorphous nature of silica at around $2\theta = 22°$. In particular, the characteristic diffractions of BSi-PEI, BSi-MAPS, and BSi-PETS were slightly shifted into lower intensity and larger angle compared to unmodified BSi. This indicated that the amine functionalization provides an insignificant change in structural properties of neat BSi filler.

Fig. 3 shows SEM images of BSi and their amine-functionalized particles. Again, amines were successfully grafted into the BSi surface. For BSi-PEI, the particles tended to be agglomerated, due to the excessive polyamine load. In contrast, other amine-functionalized BSi exhibited better grafting results (see Fig. 3c–d) without severe particle aggregation. With the lower molecular weight and shorter chain, MAPS and PETS may occupy the narrow pore in the BSi surface.

The elemental analysis results from the four fillers are shown in Table 1. The amount of N element implied the number of amino groups functionalized on the BSi particle surface. Based on the calculations, the bonded amines on BSi-PEI, BSi-MAPS, and BSi-PETS were 5.85, 1.52, and 1.24 mmol g^{-1}, respectively. In fact, one MAPS and PETS carry one amine group, whereas PEI has three amine groups. Thus, the functionalized organic chains were matched to be 1.95, 1.52, and 1.24 mmol g^{-1}, respectively.

The functionalized filler textural properties compared to their origin are listed in Table 2. Compared with pure BSi, specific surface areas, pore volumes, and pore sizes of the three modified BSi were reduced. Moreover, the BSi particles modified with PEI exhibited the lowest surface area and pore volume, which indicated the more extended amino ligands occupied more pore volume compared to MAPS and PETS.

3.2. Membrane characterization

Fig. 4 shows the FTIR spectra of prepared MMMs containing amine functionalized BSi. For the neat Pebax (NP) sample, the aliphatic −C−H stretching is observed by the sharp band at 2941 cm^{-1} and 2869 cm^{-1}. The characteristic peak of the soft polyethylene oxide (PEO) block is revealed at around 1093 cm^{-1}, attributed to the ether (C–O–C) group. Polyamide hard segment typical peaks were observed at 1637, 1732, 1541, and 3298 cm^{-1} corresponding to –C═O and −N−H stretching vibrations, respectively [24]. A broad peak indicates the hydrogen bonding between hard segments of the polymer chains at 3400-3700 cm^{-1} [10].

The amine functional groups on the BSi surface are not easily recognized in the MMM spectra due to large OH groups in the same frequency region. However, several changes in the position and intensity of polymer characteristic peaks in the IR spectra indicate the role of amine groups in polymer-inorganic filler interactions. The Si–O–Si broad peak effect of the inorganic filler in the polymer matrix is evident in the 900-1400 cm^{-1} range. Furthermore, the intensity of polyamide characteristic peaks of the MMMs at 1637, 1732, and 3298 cm^{-1} slightly decreased and shifted to a higher wavenumber after adding filler in the polymer matrix. This indicated that the interchain hydrogen bonding of the polyamide block is partially disrupted in the presence of fillers. Hydrogen bonding disruption is confirmed by a significant reduction in O–H broad peak intensity of 3400–3700 cm^{-1} in all MMMs samples.

Fig. 5 shows the surface (a-e) and cross-section (f-j) images of MMMs with different filler types. Neat Pebax membranes demonstrated smooth surfaces, indicating the polymer's complete dissolution. Micro-sized gaps were found on the surface of Pebax MMMs comprising BSi. These cavities were not observed in the cross-section image, indicating sufficient hydrogen bonding between the hydrophilic BSi sites with the Pebax backbone structure. Meanwhile, no interfacial voids were seen in the Pebax membranes with amine-functionalized BSi, as seen in Fig. 5 (c-e and h-j). Amine functional groups are believed to collide with ethylene oxides and amide chains through hydrogen bonding, narrowing the interfacial spaces between the two phases. In addition, particle aggregation might not have occurred with the assistance of the sonication step before filler incorporation into the polymer solution during the

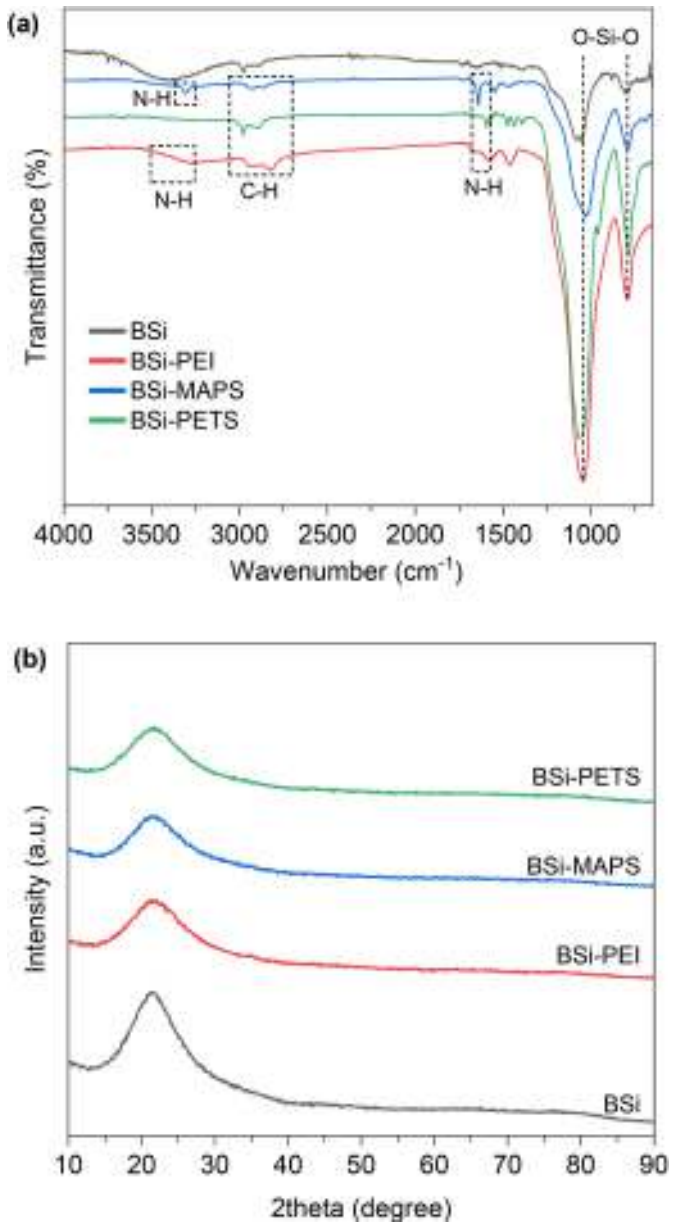

Fig. 2. FTIR spectra (a) and XRD pattern (b) of BSi and their functionalized particles.

preparation process.

Fig. 6 depicts the wide-angle X-ray diffractions of MMMs compared to their neat membrane. All membranes exhibited semi-crystalline characteristics. A broad peak at 19.62° and a less intense peak 22.50° were observed on the neat Pebax membrane, corresponding to the amorphous polyethylene oxide (PEO) soft segments and the crystalline region of the polyamide (PA) rigid part, respectively. These two peaks were shifted to a larger and stronger peak when the filler was incorporated into the Pebax matrix. With the filler addition, the Pebax membrane d-spacing decreased, indicating excellent interfacial interaction between the BSi functional groups with the polymer matrix. The rigidification effect was more significant with amine groups on the BSi surface. BSi-PEI and BSi-MAPS exhibit narrower and stronger crystalline peaks than BSi-PETS. This indicated that the amine group mixture in PEI and the secondary amine groups in MAPS would be more effective in strengthening the Pebax structure.

Fig. 7 and Table 4 represent the effects of different filler types on the decomposition temperature of the Pebax membrane. The thermal stability enhancement is related to the solid interaction between organic materials and inorganic fillers, generating a chemically bonded network structure in hybrids [9]. This interaction avoids the mobility of polymer chains resulting in higher decomposition temperature. As shown in Table 4, the decomposition temperature of all Pebax membranes could be enhanced by filler incorporation, which matched the XRD analysis result. In particular, the decomposition temperature of Pebax/BSi-PEI-10 was exceptional, significantly enhanced by increasing the filler load. However, only slight thermal stability enhancements are observed on Pebax/BSi-PETS-10. This is because the larger d-spacing values on these MMMs cannot perfectly resist polymer chain mobility during operation at high temperatures. In addition, single active amine group channels in PETS have not built up the close interaction between BSi and Pebax matrix.

DSC analysis was conducted to investigate the influence of different fillers on the glass transition temperature and melting temperature of two Pebax segments. As shown in Fig. 8 and Table 5, Pebax membranes showed the typical melting point of PE and PA segments at 14.77 °C and 204.03 °C, respectively. The glass transition temperature (T_g) was found at −52 °C (see Fig, 4–16 b). The BSi could simultaneously decrease the melting temperatures (T_m) of PE and PA blocks, showing its imperfect compatibility. Furthermore, BSi incorporation might disrupt the formation of PE and PA networks within the polymer matrix, resulting in the soft deterioration of these Pebax segments. Even though the hydrophilic characteristic of BSi was able to hook into amide and ether groups, promoting higher T_g.

Amine-modified BSi exhibited distinct impacts on the T_g and T_m of Pebax membranes. Adding BSi-PEI might disturb the formation of PA segments (lower T_m PA). Moreover, polyamine in BSi surface could strongly interact with ether groups of PE domains, resulting in higher T_m. Thus, solid rigidification consequently occurred, promoting a higher T_g value of the Pebax membrane. On the other hand, BSi-PETS exhibited a similar effect on T_g and T_m of Pebax membranes with lower rigidification magnitudes. It was because PETS with fewer amine groups than PEI could not ideally create a strong network with ether groups. In contrast, BSi-MAPS tended to rigidify the Pebax membranes by strengthening PA blocks with slight disturbance on the PE formation. This kind of reinforcement, in a way, had a significant influence on T_g improvement.

Tensile measurements were performed to study the effects of different fillers on Pebax membrane's mechanical properties. Fillers are strongly associated with the changes in Pebax's intersegmental structure. Three items were measured: Young's modulus, tensile strength, and elongation at break. Young's modulus indicates membrane brittleness, whereas tensile strength represents maximum stress before membrane break. Elongation at break implies membrane deformation resistance toward external forces. In other words, it elucidates the intersegmental chain mobility within the matrix.

Table 6 represents the effects of different filler types on Pebax membrane mechanical properties. Lower values for all mechanical properties were observed by incorporating BSi into the Pebax matrix. The BSi amorphous structure could increase membrane brittleness with a 50% reduction in Young's modulus. Moreover, since the BSi did not have a solid interfacial connection with the polymer matrix, intersegmental chain motion was inevitable. Thus, the membrane tensile strength and elongation at break became significantly degraded.

Amine functionalized BSi particles offered notable effects on Pebax membrane mechanical characteristics. BSi particles could avoid producing rugged tensile strength in the Pebax/BSi-10 membrane. This was because amine groups might enable sufficient interfacial connectivity between BSi and the Pebax matrix. Lower tensile strength was observed in Pebax/BSi-PEI-10 compared to other Pebax membranes comprising amine-functionalized BSi, due to filler agglomeration due to enormous PEI amine groups. This polyamine could strongly connect with polymer chain fragments, generating the lowest elongation at break of all other Pebax MMMs in this study. On the other hand, Pebax/BSi-PETS-10

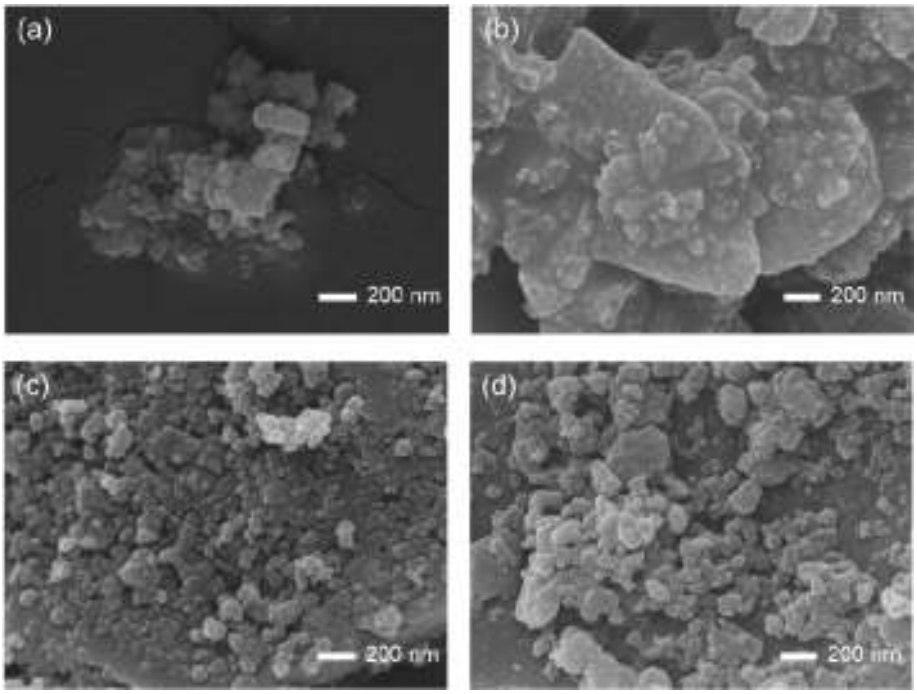

Fig. 3. Morphology of BSi (a), BSi-PEI (b), BSi-MAPS (c), and BSi-PETS (d).

Table 1
Functionalized filler organic elemental composition.

Filler type	C%	H%	N%	N (mmol g^{-1})	Org. Chain (mmol g^{-1})
BSi	0.22	0.78	0	0	0
BSi-PEI	14.40	4.00	8.19	5.85	1.95
BSi-MAPS	7.89	1.81	2.13	1.52	1.52
BSi-PETS	10.73	1.16	1.74	1.24	1.24

showed higher elongation at break value since the filler components could disturb the hard Pebax domain formation, as mentioned in the DSC analysis. At the same time BSi-PETS reinforced the Pebax soft fragments, leading to a lower Young's modulus.

3.3. Gas separation performance analysis

3.3.1. The impact of filler type on CO_2/N_2 separation of Pebax MMMs

The BSi effect and its functionalized particles on the CO_2/N_2 separation performance at 25 °C and 1 bar can be observed in Fig. 9. As depicted, the filler incorporation could upgrade CO_2 permeability due to the change in Pebax membrane interspace distance promoting a selective diffusion process. Fig. 10 showed the proposed mechanism for addressing the CO_2 transport through Pebax MMMs at different filler types. Particularly, BSi particles could enable Knudsen diffusion in Pebax MMMs. Furthermore, since BSi particles had irregular shapes and heterogenous particle size distribution, their arrangement in the Pebax matrix was found in a high tortuosity for establishing selective gas separation (as seen in Fig. 10a). Thus, the CO_2 permeability and CO_2/N_2 selectivity of Pebax membrane could be upgraded to 50% and 15%, respectively, compared to the neat Pebax membrane. In contrast, amine-functionalized BSi behaved differently compared to BSi in modifying gas transport features of the Pebax membrane (as seen in Fig. 10b). It could activate a facilitated transport mechanism, relying on reactive amine functional groups with electron-donating nitrogen to act as a Lewis base toward CO_2 molecules following the reactions below (Eqn. (5) to Eqn. (7)).

$$\underset{\textit{Primary/ secondary amine}}{R_1R_2NH} + CO_2 \rightleftarrows \underset{\text{Carbamic acid (Zwitterion)}}{R_1R_2NH^+COO^-} \tag{5}$$

$$\underset{\textit{Zwitterion}}{R_1R_2NH^+COO^-} + R_1R_2NH \rightleftarrows \underset{\textit{An ammonium carbamate}}{R_1R_2NCOO^- + R_1R_2NH_2^+} \tag{6}$$

$$\underset{\textit{Tertiary amine}}{R_1R_2R_3N} + CO_2 + H_2O \rightleftarrows \underset{\textit{An ammonium bicarbonate}}{R_1R_2R_3NH^+ + HCO_3^-} \tag{7}$$

CO_2 molecule initially reacts with a primary/secondary amine to form carbamic acid, and then the product reacts with another free amine group resulting in a carbamate molecule and $R_1R_2NH_2^+$. Since the reactions are reversible and carbamate compounds are unstable, the CO_2 molecules are desorbed completely and regenerate the filler particle surface.

Pebax/BSi-MAPS-10 showed the best CO_2 permeability and CO_2/N_2 selectivity improvement by up to 120% and 71%, respectively, compared to the neat Pebax. This improvement was also more considerable than Pebax membranes incorporating other functionalized BSi particles (PEI and PETS). Theoretically, with higher amino groups

Table 2
Filler textural properties.

Filler	BET surface area (m^2/g)	Total pore volume (cm^3/g)	Average pore width (nm)	Pore-filling fraction [1] (% v/v)
BSi	164.06	0.2169	5.44	–
BSi-PEI	0.34	0.0006	34.12	99.72
BSi-MAPS	16.61	0.0461	10.41	78.75
BSi-PETS	22.22	0.0652	11.37	69.94

[1] Comparable pore filling fractions (volume basis) relative to the neat silica.

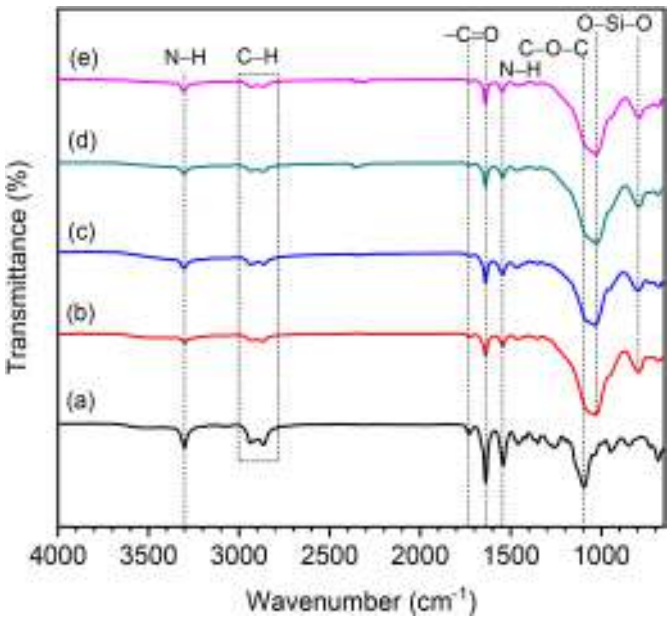

Fig. 4. FTIR spectra of prepared membranes: neat Pebax (a), Pebax/BSi-10 (b), Pebax/BSi-PEI-10 (c), Pebax/BSi-MAPS-10 (d), and Pebax/BSi-PETS-10 (e).

(primary, secondary, and tertiary) in PEI, the reactive sites become enormous, promoting high CO_2 permeability. However, excessive PEI load on the BSi surface causes severe pore blockage and particle aggregation (see Fig. 3b), impeding CO_2 diffusion concerning cross-linked alkylammonium carbamate ions on the polyamine layer [25]. Nevertheless, BSi-PEI was still good enough to improve CO_2 permeability (115%) and CO_2/N_2 selectivity (61%), slightly lower than BSi-MAPS. Larger d-spacing in Pebax/BSi-PETS-10 may contribute to unequal CO_2/N_2 separation performance compared to Pebax/BSi-PEI-10 and Pebax/BSi-MAPS-10. Besides, tertiary amine in BSi-PETS reacted with CO_2 slower than primary and secondary amines, regarding a lack of free proton to form carbamic acid. Thus, the CO_2 separation factors became slightly lower than Pebax/BSi-MAPS-10 and Pebax/BSi-PEI-10. In the case of N_2 separation, all types of filler exhibited minor enhancement for Pebax membranes. It was because this nonpolar gas had no considerable interaction with OH and NH_2 groups. Besides, the kinetic diameter of the N_2 molecule is more extensive, resulting in less diffusion rate through the Pebax matrix, and the permeability values remain unchanged.

3.3.2. *The effect of filler loading on CO_2/N_2 separation of Pebax/BSi-MAPS*

Fig. 11 depicts the CO_2/N_2 separation performance of Pebax MMMs with increasing BSi-MAPS loading. The CO_2 permeability and CO_2/N_2 selectivity initially inclined with increasing BSi-MAPS content up to 10 wt%, then dropped back at a higher load. Particle aggregation is ascribed to higher BSi-MAPS content. Larger particle sizes and low surface area might contribute to poor filler dispersion at higher concentrations. Thus, the optimum BSi-MAPS load for preparing Pebax MMMs should be 10 wt%.

3.3.3. *The effect of pressure on CO_2/N_2 separation of Pebax/BSi-MAPS*

Fig. 12 displays the pressure effect on gas permeate flux and separation performance of Pebax/BSi-MAPS-10 at 25 °C and 1 bar. As shown in Fig. 12a, the CO_2 permeate flow rate rose from 0.010 to 0.0227 scm^3/min with elevating pressure (1–5 bar), following a linear trend suitable for practical applications. Moreover, the Pebax MMM CO_2 permeability decreased with increasing feed gas pressure (as shown in Fig. 12b), indicating that CO_2 permeation through the membrane follows a facilitated transport mechanism. The decreasing trend was evident from 1 to 2 bar of pressure and unchanged at high feed gas pressure because of

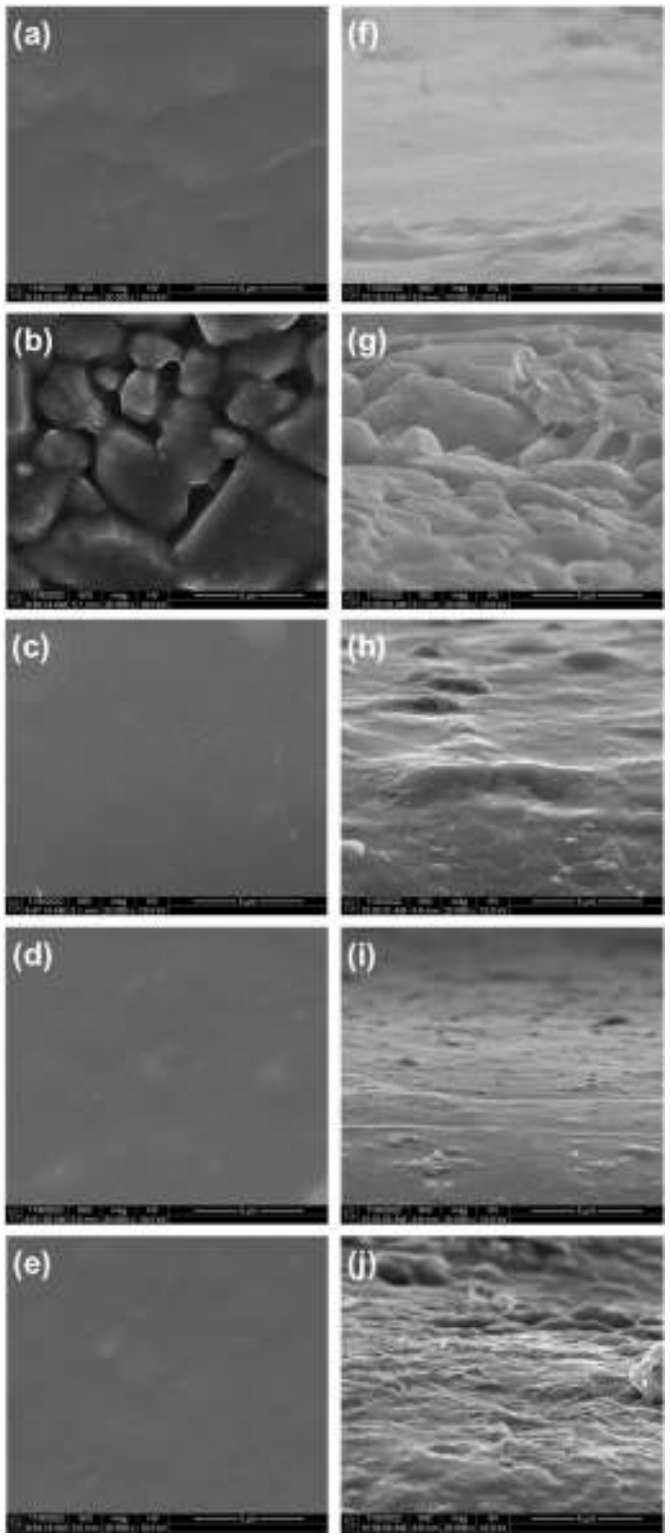

Fig. 5. The FE-SEM surface (a–e) and cross-section (f–j) images of pure Pebax membrane (a and f) and their MMMs with different fillers: BSi-10 (b and g), BSi-PEI-10 (c and h), BSi-MAPS-10 (d and i), and BSi-PETS-10 (e and j).

CO_2 adsorption saturation and membrane compaction. It implied that the other two mechanisms, such as solution-diffusion and Knudsen diffusion, still existed during the separation process, leading to an inclining trend in permeate flow rate (as indicated in Fig. 10). Nevertheless, since these two transport mechanisms were found in a smaller portion than facilitated transport, hence, it could not significantly

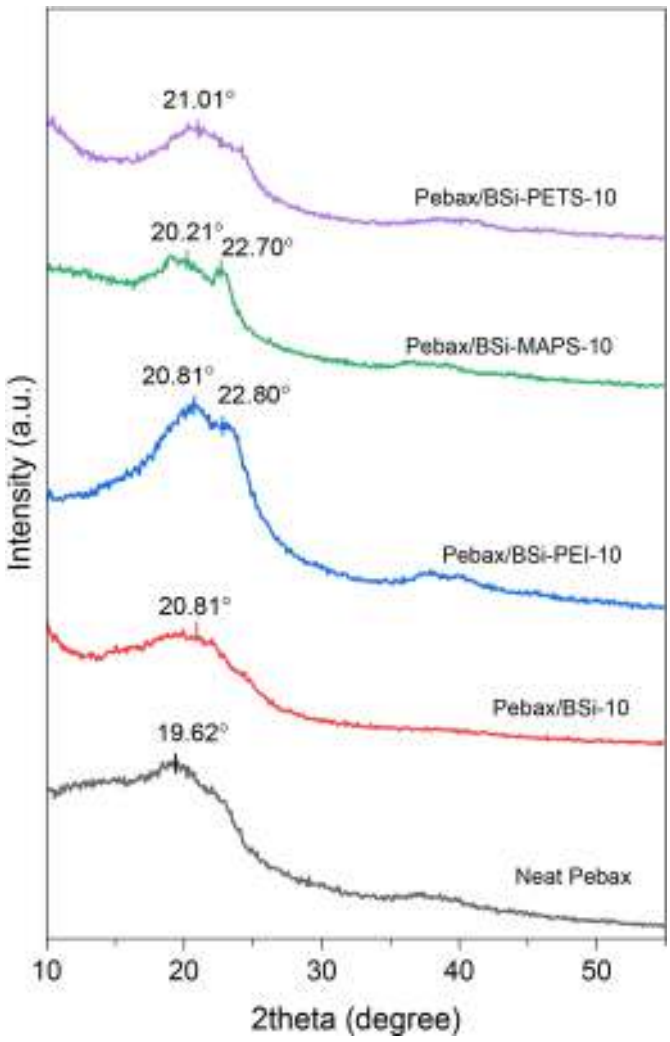

Fig. 6. X-ray diffraction pattern of Pebax MMMs with different BSi particles.

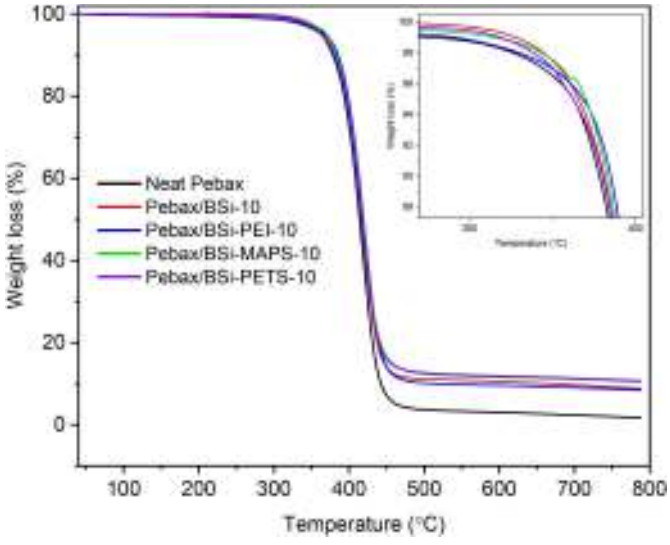

Fig. 7. TGA curve comparison of prepared membranes.

enhance CO_2 permeability at pressurized condition (4–5 bar). In other words, the CO_2-carrier reaction product concentration attains the maximum value and becomes constant. Specifically, a further increase in the partial pressure of CO_2 would not remarkably increase the CO_2-carrier reaction product concentration. In contrast, the decreasing permeability trend with increasing pressure was not found in N_2 gas. Instead, it indicated that the N_2 separation performance could be maintained at stable conditions even under pressurized conditions.

Table 4
Prepared membrane decomposition temperature.

Sample	T_{onset} (°C)	DTG_{max} (°C)
Neat Pebax	385.34	417.37
Pebax/BSi-10	387.07	416.78
Pebax/BSi-PEI-10	388.98	420.65
Pebax/BSi-MAPS-10	388.29	420.00
Pebax/BSi-PETS-10	387.25	417.86

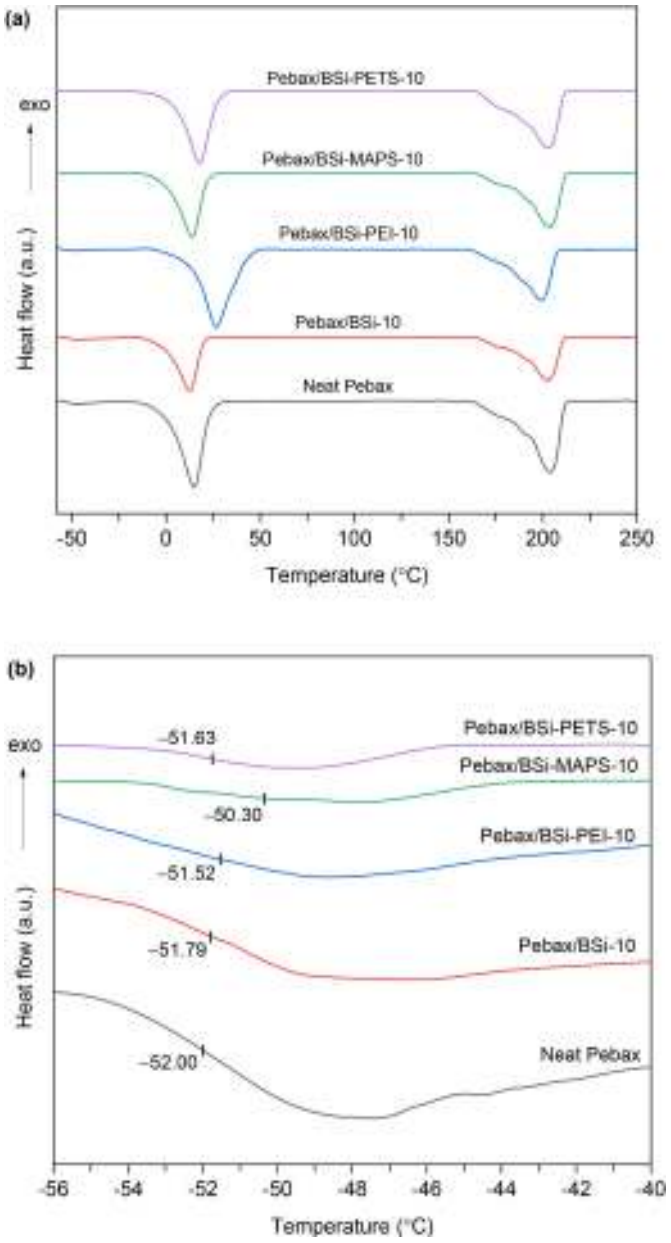

Fig. 8. DSC results for prepared Pebax MMMs with different fillers: 60 to 250 °C (a) and −56 to −40 °C.

3.3.4. Durability test of Pebax/BSi-MAPS-10

Membrane durability is prominent to intensify the prospect for

Table 5
DSC analysis of prepared Pebax MMMs.

Sample	T_g (°C)	T_m PE (°C)	T_m PA (°C)
Neat Pebax	−52.00	14.77	204.03
Pebax/BSi-10	−51.79	12.63	202.42
Pebax/BSi-PEI-10	−51.52	26.77	199.07
Pebax/BSi-MAPS-10	−50.30	13.78	204.07
Pebax/BSi-PETS-10	−51.63	17.79	203.49

Table 6
Mechanical properties of Pebax MMMs with different fillers[a].

Sample	Tensile strength (MPa)	Elongation at break (%)	Young's modulus (MPa)
Neat Pebax	106.02	260.45	664.86
Pebax/BSi-10	56.49	148.12	342.00
Pebax/BSi-PEI-10	62.58	30.28	537.58
Pebax/BSi-MAPS-10	82.28	56.82	929.48
Pebax/BSi-PETS-10	83.90	299.38	513.13

[a] The results were the average of triplicate testing with a standard deviation below ±30%.

industrial applications. Accordingly, a durability test was performed under three days of continuous operation at ambient temperatures and 1 bar of pressure. The test was subjected to Pebax membrane containing 10 wt% BSi-MAPS as the best MMM in this study. As a result, CO_2 permeability and CO_2/N_2 selectivity were relatively stable for three days of continuous operation testing with reasonable fluctuation (Fig. 13). The minimum drops were observed at 54–60 h operation time with 88 Barrer in CO_2 permeability and 99 in CO_2/N_2 selectivity. At the end of testing, CO_2 permeability and CO_2/N_2 selectivity remained unchanged at 89 Barrer and 100, respectively.

3.3.5. Benchmarking of prepared Pebax MMMs with recent studies

Fig. 14 compares CO_2/N_2 separation performances for Pebax comprising amine functionalized BSi in this work and available Pebax MMMs from previous research. BSi (10 wt%) could not significantly upgrade CO_2 permeability and CO_2/N_2 selectivity, only exhibiting 0.44 of PER-CO_2 and 0.12 of SeER-CO_2/N_2, which was insufficient to exceed

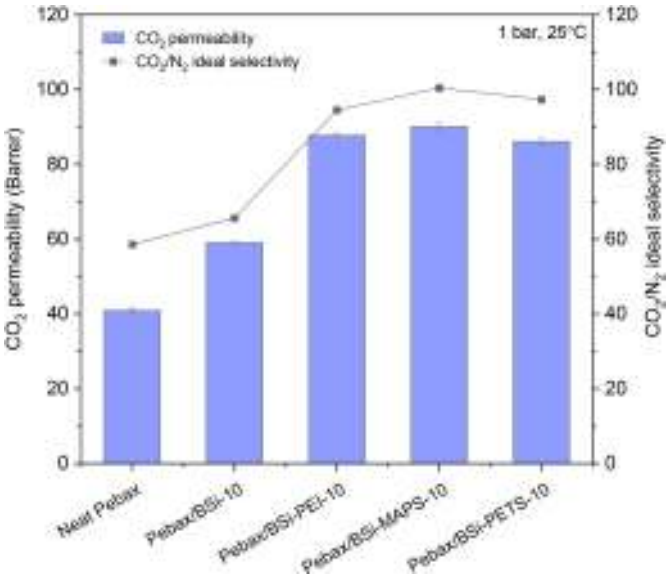

Fig. 9. Pebax MMM CO_2/N_2 separation performance with different types of fillers.

Table 7
CO_2/N_2 separation performance comparison of Pebax MMMs in this study with literature.

Membrane sample	Filler loading (wt%)	T/P (°C/bar)	P–CO_2 (Barrer)	α-CO_2/N_2	PER-CO_2[a]	SeER-CO_2/N_2[a]	Reference
Pebax/BSi-10	10	25/1	59.02	65.64	0.44	0.12	This study
Pebax/BSi-PEI	10	25/1	87.73	94.49	1.15	0.61	
Pebax/BSi-MAPS	10	25/1	90.02	100.41	1.20	0.71	
Pebax/BSi-PETS	10	25/1	86.10	97.32	1.11	0.66	
Pebax MMMs with silica-based fillers							
Pebax/SiO_2-rice straw	2	30/7	270	4.12	11.27	1.00	[12]
Pebax/MCM-41	20	25/1	138	53	0.68	−0.02	[16]
Pebax/MCM-41-PEI	20	25/1	112	57	0.37	0.06	[16]
Pebax/PVC/SiO_2-IL	8	25/1	124	76	0.63	0.35	[26]
Pebax/PVC/SiO_2-OB	8	25/1	107	61	0.41	0.09	[26]
Pebax/FS7	10	25/8	56.96	98.21	0.67	0.04	[27]
Pebax/FS16	10	25/8	58.46	71.29	0.71	−0.25	[27]
Pebax/SiO_2	1	25/4	73.65	81.82	1.20	0.40	[28]
Pebax/NOHMs-120	15	25/2	246.7	66.4	2.67	0.76	[33]
Pebax/SiO_2@PPy	1	35/2	274	40.1	1.14	0.04	[36]
Recent Pebax MMMs							
Pebax/ZIF-8[b]	8	25/4	73.3	82.0	0.28	2.5	[30]
Pebax/maltitol/ZIF-8	10	30/10	429.57	69.31	0.25[c]	0.04[c]	[35]
Pebax/ZIF-94	10	35/3	157	27.5	0.67	−0.05	[31]
Pebax/ZIF-67-L	10	30/2	91.59	51.74	0.74	0.24	[32]
Pebax/arg@GO	0.4	25/1	169	70	0.63[c]	1.26[c]	[37]
Pebax/PEI@ZIF HNTS	7	25/2	177	72	0.40[c]	0.11[c]	[34]
Pebax/ZCN	8	25/2	110.5	84.4	0.60	0.12	[38]
Pebax/CuBTC-IL	15	35/1	335	176	1.12	4.5	[2]
Pebax/CuBDC@MoS_2	2.5	–	123	69	0.43	0.81	[39]
Pebax/MIL-178(Fe)	5	35/3	312	25	0.12	0.25	[29]
Pebax-1657/$Ti_3C_2T_x$	0.5	25/4	70.24	93.18	0.15	0.68	[40]
Pebax-1657/γ-Al_2O_3- IL	10	25/7	126.79	102.36	0.47	1.24	[41]

[a] Based on the performance of pure Pebax membranes.
[b] In-situ growth filler.
[c] Based on the performance of modified Pebax membranes. PER: Permeability enhancement ratio, SeER: Selectivity enhancement ratio, IL: hydrophilic, OB: hydrophobic, FS: fumed silica, NOHMs: silica nanoparticle organic hybrid materials, PPy: polypyrrole., arg: arginine, IL: ionic liquid, ZCN: ZIF-90@C_3N_4, HNTs: 1D nanotubes, ZIF-67-L: leaf-like hierarchical ZIF-67.

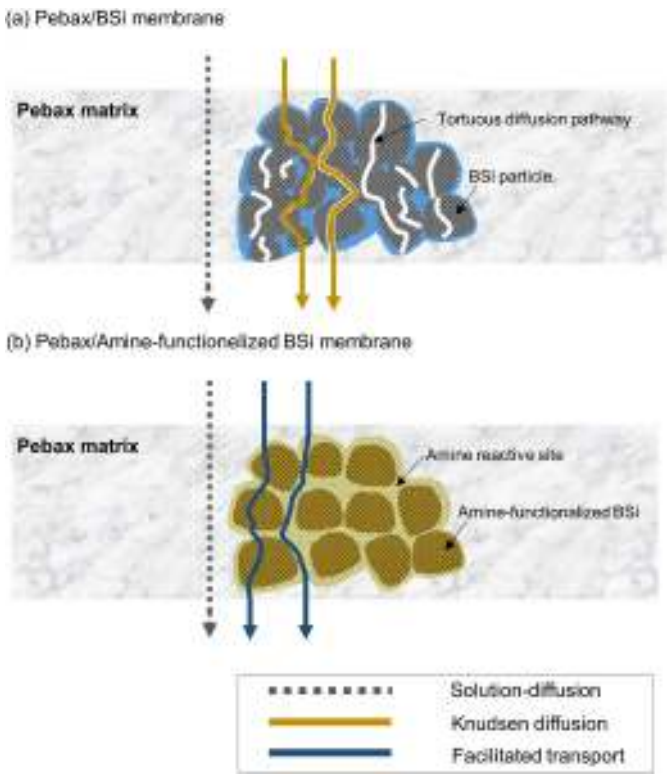

Fig. 10. Illustration of proposed CO_2 transport through Pebax MMMs at different filler types.

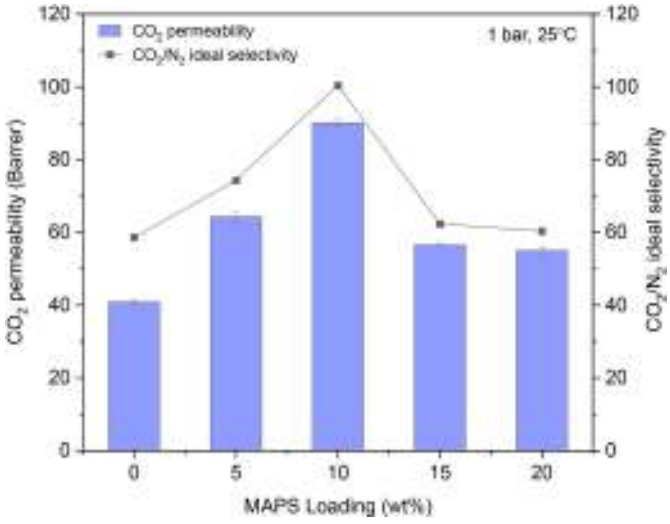

Fig. 11. CO_2/N_2 separation performance of MMMs at different BSi-MAPS loading.

Robeson's upper bound 2008. It matched the CO_2/N_2 separation performance of some Pebax MMMs comprising unmodified silica particles, such as Pebax/2% SiO_2 rice straw [12], Pebax/20% MCM-41 [16], Pebax/PVC/8% SiO_2-OB [26], Pebax/10% FS16 [27], and Pebax/SiO_2 1% [28]. These unmodified silica nanoparticles could only significantly impact CO_2 permeability by altering Pebax chain packing with advantageous diffusion gas pathways. CO_2/N_2 selectivity, however, was insignificantly upgraded concerning the lack of reactive sites on the filler surfaces to provide a CO_2-selective separation process. This phenomenon was also observed in recent Pebax membranes with metal-organic frameworks (MOFs) filler such as Pebax/5% MIL-178

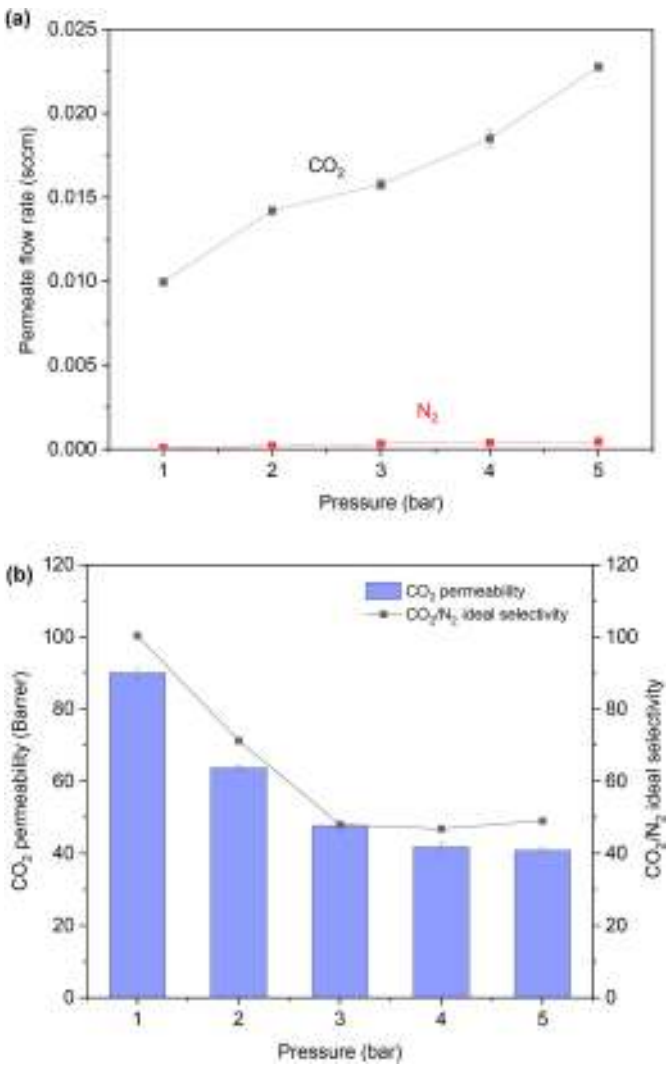

Fig. 12. Feed pressure effect on (a) permeation fluxes; (b) Pebax/BSi-MAPS-10 membrane CO_2/N_2 separation performance.

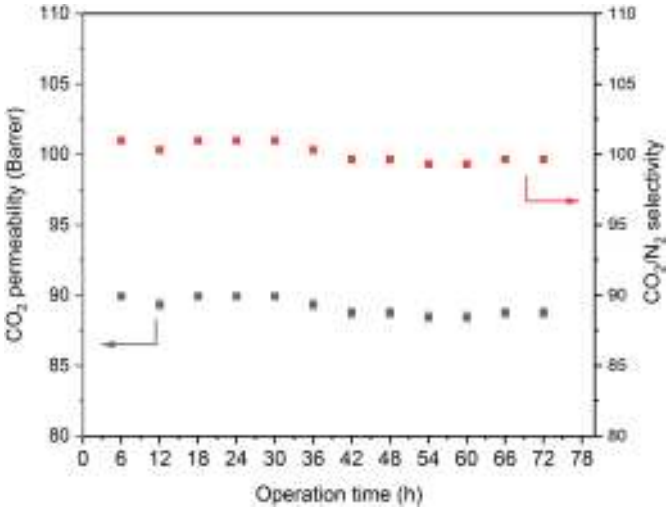

Fig. 13. Pebax MMM long-term stability with 10 wt% MAPS load.

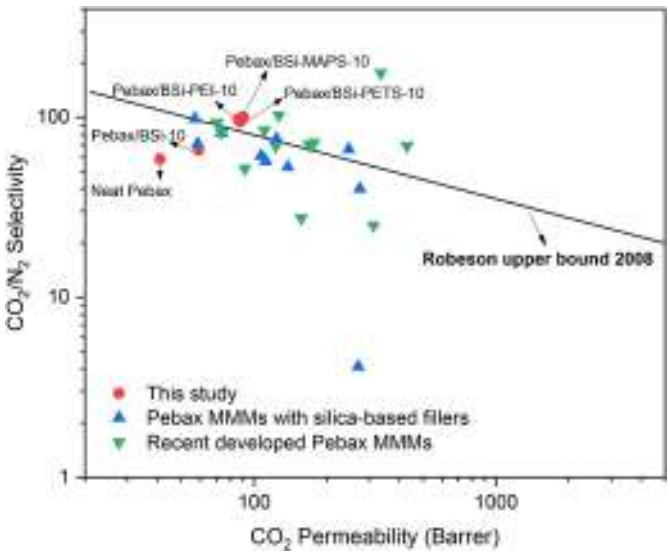

Fig. 14. The ideal CO_2/N_2 separation performances of prepared Pebax membranes in this study compared to Pebax-based membranes reported in the literature, plotted from Table 7.

[29], Pebax/8% ZIF-8 [30], Pebax/10% ZIF-94 [31], and Pebax/10% ZIF-67-L [32].

Incorporating amine functionalized BSi could eventually overcome the neat Pebax membrane trade-off problem. The PER-CO_2 of Pebax MMMs containing 10 wt% functionalized BSi ranged from 1.10 to 1.50, while their SeER-CO_2/N_2 varied from 0.61 to 0.71. The CO_2 permeability and CO_2/N_2 selectivity values were relatively balanced at 60–90 Barrer and 70–100, respectively. These performances were superior among available Pebax MMMs with silica-based fillers and comparable with the other Pebax MMMs with functionalized fillers in the literature. Nonetheless, the CO_2 permeability values in this study were lower than other reported high-performance Pebax MMMs. For instance, a Pebax/modified silica membrane, Pebax/NOHMs-120, exhibited 246.7 Barrer of CO_2 permeability (PER-CO_2 = 2.67) at 15 wt% filler loading [33]. It was almost thrice bigger than Pebax/BSi-MAPS-10 in this study. Other Pebax MMMs with modified MOF fillers, such as Pebax/CuBTC-IL [2], Pebax/PEI@ZIF HNTS [34], and Pebax/maltitol/ZIF-8 [35], also revealed notable CO_2 permeability, 2–5 times higher than the best Pebax MMMs in this study. Pebax/CuBTC-IL was also superior in CO_2/N_2 selectivity (176) with 450% enhancement from its pure Pebax membrane. Therefore, further development of functionalized BSi in this study is still needed to obtain much higher CO_2 permeability and CO_2/N_2 selectivity, regardless of the trade-off issue extermination.

4. Conclusion

BSi derived from rice husk was successfully functionalized with three different amines (PEI, MAPS, and PETS) and incorporated into Pebax to fabricate MMMs. PEI, which carried multiple amino groups, showed high occupancy to fill into the BSi pore surface, providing immense CO_2 reactive sites. Incorporating amine-functionalized BSi was favorable to decreasing the interfacial space (d-spacing) and increasing the thermal stability of prepared Pebax MMMs. It was primarily due to strong interfacial interaction between amine or hydroxyl groups (in original BSi particles) with the core Pebax polymer intersegmental chains. The amine groups in BSi could effectively enable a facilitated transport mechanism through the Pebax membranes. BSi-MAPS was shown to be the best filler for Pebax in this study due to sufficient amine occupancy and reactive CO_2 sites on the BSi surface, with 90.05 Barrer of CO_2 permeability and 100.41 CO_2/N_2 selectivity. To further improve these Pebax MMMs, tuning the pore structure of the original BSi should be considered to enlarge amine occupancy, avoiding severe pore blockage and particle aggregation. The CO_2/N_2 separation performance can be improved or even expanded to any other polar/nonpolar gas pair separation.

Credit author statement

Wahyu Kamal Setiawan: Conceptualization; Writing - original draft; Writing - review & editing. Kung-Yuh Chiang: Methodology; Reviewing; Revising; Supervising.

Declaration of competing interest

The authors declare that they have no known competing financial interests or personal relationships that could have appeared to influence the work reported in this paper.

Data availability

The data that has been used is confidential.

Acknowledgment

The authors thank the Taiwan Ministry of Science and Technology (MOST) (MOST-109-2221-E-008-023-MY2) for financially supporting this work.

References

[1] R. Lindsey, Climate Change: Atmospheric Carbon Dioxide, 2022. https://www.climate.gov/news-features/understanding-climate/climate-change-atmospheric-carbon-dioxide. (Accessed 23 November 2022), 2022.
[2] N. Habib, O. Durak, M. Zeeshan, A. Uzun, S. Keskin, A novel IL/MOF/polymer mixed matrix membrane having superior CO_2/N_2 selectivity, J. Membr. Sci. 658 (2022), 120712, https://doi.org/10.1016/j.memsci.2022.120712.
[3] G.V. Sarrigani, J. Ding, A.E. Ghadi, D. Alam, P. Fitzgerald, D.E. Wiley, D.K. Wang, Interfacially-confined polyetherimide tubular membranes for H_2, CO_2 and N_2 separations, J. Membr. Sci. 655 (2022), 120596, https://doi.org/10.1016/j.memsci.2022.120596.
[4] C. Jiao, Z. Li, X. Li, M. Wu, H. Jiang, Improved CO_2/N_2 separation performance of Pebax composite membrane containing polyethyleneimine functionalized ZIF-8, Sep. Purif. Technol. 259 (2021), 118190, https://doi.org/10.1016/j.seppur.2020.118190.
[5] F. Pazani, A. Aroujalian, Enhanced CO_2-selective behavior of Pebax-1657: a comparative study between the influence of graphene-based fillers, Polym. Test. 81 (2020), 106264, https://doi.org/10.1016/j.polymertesting.2019.106264.
[6] K.C. Wong, P.S. Goh, A.F. Ismail, Enhancing hydrogen gas separation performance of thin film composite membrane through facilely blended polyvinyl alcohol and PEBAX, Int. J. Hydrogen Energy 46 (37) (2021) 19737–19748, https://doi.org/10.1016/j.ijhydene.2020.09.079.
[7] D.J. Harrigan, J. Yang, B.J. Sundell, J.A. Lawrence, J.T. O'Brien, M.L. Ostraat, Sour gas transport in poly(ether-b-amide) membranes for natural gas separations, J. Membr. Sci. 595 (2020), 117497, https://doi.org/10.1016/j.memsci.2019.117497.
[8] M. Isanejad, N. Azizi, T. Mohammadi, Pebax membrane for CO_2/CH_4 separation: effects of various solvents on morphology and performance, J. Appl. Polym. Sci. 134 (9) (2017), https://doi.org/10.1002/app.44531.
[9] W.K. Setiawan, K.Y. Chiang, Silica applied as mixed matrix membrane inorganic filler for gas separation: a review, Sustainable Environment Research 29 (1) (2019) 32, https://doi.org/10.1186/s42834-019-0028-1.
[10] M. Isanejad, T. Mohammadi, Effect of amine modification on morphology and performance of poly (ether-block-amide)/fumed silica nanocomposite membranes for CO_2/CH_4 separation, Mater. Chem. Phys. 205 (2018) 303–314, https://doi.org/10.1016/j.matchemphys.2017.11.018.
[11] A.L. Khan, C. Klaysom, A. Gahlaut, A.U. Khan, I.F.J. Vankelecom, Mixed matrix membranes comprising of Matrimid and $-SO_3H$ functionalized mesoporous MCM-41 for gas separation, J. Membr. Sci. 447 (2013) 73–79, https://doi.org/10.1016/j.memsci.2013.07.011.
[12] M. Bhattacharya, M.K. Mandal, Synthesis of rice straw extracted nano-silica-composite membrane for CO_2 separation, J. Clean. Prod. 186 (2018) 241–252, https://doi.org/10.1016/j.jclepro.2018.03.099.
[13] A.A. Ghazali, S. Abd Rahman, R. Abu Samah, Preparation and characterisation of pineapple peel waste as nanoadsorbent incorporated into Pebax 1657 nanocomposite membrane for CO_2/CH_4 separation, Mater. Today: Proc. 41 (2021) 88–95, https://doi.org/10.1016/j.matpr.2020.11.1012.
[14] N. Waheed, A. Mushtaq, S. Tabassum, M.A. Gilani, A. Ilyas, F. Ashraf, Y. Jamal, M. R. Bilad, A.U. Khan, A.L. Khan, Mixed matrix membranes based on polysulfone and

rice husk extracted silica for CO_2 separation, Sep. Purif. Technol. 170 (2016) 122–129, https://doi.org/10.1016/j.seppur.2016.06.035.
[15] W.K. Setiawan, K.Y. Chiang, Crop residues as potential sustainable precursors for developing silica materials: a review, Waste and Biomass Valorization 12 (5) (2021) 2207–2236, https://doi.org/10.1007/s12649-020-01126-x.
[16] H. Wu, X. Li, Y. Li, S. Wang, R. Guo, Z. Jiang, C. Wu, Q. Xin, X. Lu, Facilitated transport mixed matrix membranes incorporated with amine functionalized MCM-41 for enhanced gas separation properties, J. Membr. Sci. 465 (2014) 78–90, https://doi.org/10.1016/j.memsci.2014.04.023.
[17] S. Meshkat, S. Kaliaguine, D. Rodrigue, Mixed matrix membranes based on amine and non-amine MIL-53(Al) in Pebax® MH-1657 for CO_2 separation, Sep. Purif. Technol. 200 (2018) 177–190, https://doi.org/10.1016/j.seppur.2018.02.038.
[18] R. Ding, W. Zheng, K. Yang, Y. Dai, X. Ruan, X. Yan, G. He, Amino-functional ZIF-8 nanocrystals by microemulsion based mixed linker strategy and the enhanced CO_2/N_2 separation, Sep. Purif. Technol. 236 (2020), 116209, https://doi.org/10.1016/j.seppur.2019.116209.
[19] C. Song, R. Li, Z. Fan, Q. Liu, B. Zhang, Y. Kitamura, CO_2/N_2 separation performance of Pebax/MIL-101 and Pebax/NH_2-MIL-101 mixed matrix membranes and intensification via sub-ambient operation, Sep. Purif. Technol. 238 (2020), 116500, https://doi.org/10.1016/j.seppur.2020.116500.
[20] W.K. Setiawan, K.Y. Chiang, Eco-friendly rice husk pre-treatment for preparing biogenic silica: gluconic acid and citric acid comparative study, Chemosphere 279 (2021), 130541, https://doi.org/10.1016/j.chemosphere.2021.130541.
[21] G.P. Knowles, A.L. Chaffee, Aminopropyl-functionalized silica CO_2 adsorbents via sonochemical methods, J. Chem. (2016), 1070838, https://doi.org/10.1155/2016/1070838, 2016.
[22] R. Ellerbrock, M. Stein, J. Schaller, Comparing amorphous silica, short-range-ordered silicates and silicic acid species by FTIR, Sci. Rep. 12 (1) (2022), 11708, https://doi.org/10.1038/s41598-022-15882-4.
[23] H. Liu, H. Yu, P. Jin, M. Jiang, G. Zhu, Y. Duan, Z. Yang, H. Qiu, Preparation of mesoporous silica materials functionalized with various amino-ligands and investigation of adsorption performances on aromatic acids, Chem. Eng. J. 379 (2020), 122405, https://doi.org/10.1016/j.cej.2019.122405.
[24] F. Dorosti, A. Alizadehdakhel, Fabrication and investigation of PEBAX/Fe-BTC, a high permeable and CO_2 selective mixed matrix membrane, Chem. Eng. Res. Des. 136 (2018) 119–128, https://doi.org/10.1016/j.cherd.2018.01.029.
[25] L.B. Hamdy, C. Goel, J.A. Rudd, A.R. Barron, E. Andreoli, The application of amine-based materials for carbon capture and utilisation: an overarching view, Materials Advances 2 (18) (2021) 5843–5880, https://doi.org/10.1039/D1MA00360G.
[26] A. Kargari, H. Sanaeepur, Khalilinejad, Preparation and characterization of (Pebax 1657 + silica nanoparticle)/PVC mixed matrix composite membrane for CO_2/N_2 separation, Chem. Pap. 71 (4) (2017) 803–818, https://doi.org/10.1007/s11696-016-0084-5.
[27] Z. Aghaei, L. Naji, V. Hadadi Asl, G. Khanbabaei, F. Dezhagah, The influence of fumed silica content and particle size in poly (amide 6-b-ethylene oxide) mixed matrix membranes for gas separation, Sep. Purif. Technol. 199 (2018) 47–56, https://doi.org/10.1016/j.seppur.2018.01.035.
[28] M. Salehi Maleh, A. Raisi, Comparison of porous and nonporous filler effect on performance of poly (ether-block-amide) mixed matrix membranes for gas separation applications, Chem. Eng. Res. Des. 147 (2019) 545–560, https://doi.org/10.1016/j.cherd.2019.05.038.
[29] M.R. Hasan, H. Zhao, N. Steunou, C. Serre, M. Malankowska, C. Téllez, J. Coronas, Optimization of MIL-178(Fe) and Pebax® 3533 loading in mixed matrix membranes for CO_2 capture, Int. J. Greenh. Gas Control 121 (2022), 103791, https://doi.org/10.1016/j.ijggc.2022.103791.
[30] M.S. Maleh, A. Raisi, In-situ growth of ZIF-8 nanoparticles in Pebax-2533 for facile preparation of high CO_2-selective mixed matrix membranes, Colloids Surf. A Physicochem. Eng. Asp. 659 (2023), 130747, https://doi.org/10.1016/j.colsurfa.2022.130747.
[31] M. Rafiul Hasan, A. Moriones, M. Malankowska, J. Coronas, Study on the recycling of zeolitic imidazolate frameworks and polymer Pebax® 1657 from their mixed matrix membranes applied to CO_2 capture, Sep. Purif. Technol. 304 (2023), 122355, https://doi.org/10.1016/j.seppur.2022.122355.
[32] Q. Zhao, S. Lian, R. Li, Y. Yang, G. Zang, C. Song, Fabricating Leaf-like hierarchical ZIF-67 as Intra-Mixed matrix membrane microarchitecture for efficient intensification of CO_2 separation, Sep. Purif. Technol. 305 (2023), 122460, https://doi.org/10.1016/j.seppur.2022.122460.
[33] D. Wang, S. Song, W. Zhang, Z. He, Y. Wang, Y. Zheng, D. Yao, Y. Pan, Z. Yang, Z. Meng, Y. Li, CO_2 selective separation of Pebax-based mixed matrix membranes (MMMs) accelerated by silica nanoparticle organic hybrid materials (NOHMs), Sep. Purif. Technol. 241 (2020), 116708, https://doi.org/10.1016/j.seppur.2020.116708.
[34] R. Ding, Q. Wang, X. Ruan, Y. Dai, X. Li, W. Zheng, G. He, Novel and versatile PEI modified ZIF-8 hollow nanotubes to construct CO_2 facilitated transport pathway in MMMs, Sep. Purif. Technol. 289 (2022), 120768, https://doi.org/10.1016/j.seppur.2022.120768.
[35] D. Nobakht, R. Abedini, A new ternary Pebax®1657/maltitol/ZIF-8 mixed matrix membrane for efficient CO_2 separation, Process Saf. Environ. Protect. 170 (2023) 709–719, https://doi.org/10.1016/j.psep.2022.12.058.
[36] X. Wang, X. Ding, H. Zhao, J. Fu, Q. Xin, Y. Zhang, Pebax-based mixed matrix membranes containing hollow polypyrrole nanospheres with mesoporous shells for enhanced gas permeation performance, J. Membr. Sci. 602 (2020), 117968, https://doi.org/10.1016/j.memsci.2020.117968.
[37] Z. Chen, P. Zhang, H. Wu, S. Sun, X. You, B. Yuan, J. Hou, C. Duan, Z. Jiang, Incorporating amino acids functionalized graphene oxide nanosheets into Pebax membranes for CO_2 separation, Sep. Purif. Technol. 288 (2022), 120682, https://doi.org/10.1016/j.seppur.2022.120682.
[38] F. Guo, D. Li, R. Ding, J. Gao, X. Ruan, X. Jiang, G. He, W. Xiao, Constructing MOF-doped two-dimensional composite material ZIF-90@C_3N_4 mixed matrix membranes for CO_2/N_2 separation, Sep. Purif. Technol. 280 (2022), 119803, https://doi.org/10.1016/j.seppur.2021.119803.
[39] N. Liu, J. Cheng, W. Hou, C. Yang, X. Yang, J. Zhou, Bottom-up synthesis of two-dimensional composite via CuBDC-ns growth on multilayered MoS_2 to boost CO_2 permeability and selectivity in Pebax-based mixed matrix membranes, Sep. Purif. Technol. 282 (2022), 120007, https://doi.org/10.1016/j.seppur.2021.120007.
[40] W. Guan, X. Yang, C. Dong, X. Yan, W. Zheng, Y. Xi, X. Ruan, Y. Dai, G. He, Prestructured MXene fillers with uniform channels to enhance CO_2 selective permeation in mixed matrix membranes, J. Appl. Polym. Sci. 138 (8) (2021), 49895, https://doi.org/10.1002/app.49895.
[41] M.E. Kojabad, A. Babaluo, A. Tavakoli, R.L.M. Sofla, H.G. Kahnamouei, Comparison of acidic and basic ionic liquids effects on dispersion of alumina particles in Pebax composite membranes for CO_2/N_2 separation: experimental study and molecular simulation, J. Environ. Chem. Eng. 9 (5) (2021), 106116, https://doi.org/10.1016/j.jece.2021.106116.